

Article

Microstructure and Mechanical Properties of Fly Ash-Based Geopolymer Cementitious Composites

Guanglong Yu and Yanmin Jia *

School of Civil Engineering, Northeast Forestry University, Harbin 150040, China; yuguanglong@nefu.edu.cn
* Correspondence: jiayanmin@nefu.edu.cn; Tel.: +86-(451)-8219-1972

Abstract: In this paper, the microstructure, mechanical properties, and preparation of geopolymer were investigated. The effects of the proportion of slag and fly ash, the modulus of water glass, and the water–binder ratio on the microstructure, mechanical properties, and preparation of geopolymer were analyzed. The research content of this paper is as follows: Taking the 7-day and 28-day compressive strength and flexural strength of the geopolymer specimens as the evaluation criteria, considering the proportion of slag and fly ash, the modulus of water glass, and the water–binder ratio, the three factors and five levels are respectively considered for a total of 25 sets of orthogonal experiments. Through the range analysis and variance analysis, the influence of each factor on the mechanical properties was analyzed, and the best mix ratio was obtained. Using scanning electron microscope and X-ray diffraction analysis and other testing methods, the mechanical properties, microstructure, and phase composition of geopolymers under the influence of various factors were studied and analyzed.

Keywords: geopolymer; mechanical properties; microstructure analysis



Citation: Yu, G.; Jia, Y. Microstructure and Mechanical Properties of Fly Ash-Based Geopolymer Cementitious Composites. *Minerals* **2022**, *12*, 853. <https://doi.org/10.3390/min12070853>

Academic Editors: Thomas N. Kerestedjian and Alexander Karamanov

Received: 17 May 2022

Accepted: 21 June 2022

Published: 4 July 2022

Publisher's Note: MDPI stays neutral with regard to jurisdictional claims in published maps and institutional affiliations.



Copyright: © 2022 by the authors. Licensee MDPI, Basel, Switzerland. This article is an open access article distributed under the terms and conditions of the Creative Commons Attribution (CC BY) license (<https://creativecommons.org/licenses/by/4.0/>).

1. Introduction

Geopolymers are known as a new environmentally friendly inorganic cementitious material within the material field [1,2], and have been a popular research topic worldwide in recent decades. The initial geopolymer experimental research only used mineral materials such as metakaolin but, as a result of the advancement of the industrial process and the progress of research, the raw materials of geopolymers have also increased. Materials such as industrial solid waste and construction waste such as red mud have been used as the raw materials of geopolymers. The main components of these industrial solid wastes and construction wastes are basically the same as those of the mineral raw materials such as metakaolin, which are silicates or aluminosilicates, and high-performance geopolymers can also be prepared. Some studies have shown that the properties of calcined industrial solid waste result in mechanical properties of geopolymers prepared from fly ash, slag, and calcined kaolin that are superior to those of naturally formed mineral raw materials such as uncalcined kaolin and clay prepared geopolymers [3]. Geopolymers are also known as mineral polymers, soil polymers, etc. [4]. The raw material sources are pozzolanic activity or industrial solid wastes such as slag, fly ash, coal gangue, and red mud, in addition to zeolite and metakaolin. The excitation effect of the hard aluminosilicate raw material results in the formation of a three-dimensional network aluminosilicate mineral composed of a silicon-oxygen tetrahedron and aluminum-oxygen tetrahedron as the skeleton.

The activator is one of the important components of geopolymers, and can be divided into acidic and basic forms. Research on alkali excitation technology is in its early stages and the research level is relatively mature [5]. The alkali excitation agent is considered to be able to react with Ca^{2+} to form soluble or insoluble and anion or anionic chemical compositions [6,7]. The strong alkaline activator can not only provide soluble silicate ions, but also promote the rapid dissolution of Si and Al in the aluminosilicate raw materials

and the formation of bonds such as Si-O-Al and Si-O-Al-O. Among these, caustic alkali (NaOH, KOH), sodium water glass ($\text{Na}_2\text{O}\cdot n\text{SiO}_2$), potassium water glass ($\text{K}_2\text{O}\cdot n\text{SiO}_2$), or the above-mentioned mixed solutions are adopted by the majority of researchers because of their low price and easy availability.

As a result of the advancement in the industrial process, the selection of geopolymer raw materials has tended to develop from traditional materials such as clay, metakaolin, zeolite, and feldspar, to industrial solid wastes such as fly ash, slag, and tailings [6,8–10]. This has a direct impact on the properties of geopolymers, and the research level of geopolymers has risen to a new level.

Fly ash is an industrial by-product from coal-fired power generation and steam production. Fly ash and lime ($\text{Ca}(\text{OH})_2$) react with water to form the same compound as cement. As a widely recognized building material, its application as a concrete, mortar, and slurry admixture is of great significance to the concrete industry [11–14], and it can be rationally utilized as a geopolymer raw material. There is an amorphous phase in fly ash that eventually reacts with the hydration product and crystalline impurities. Statistics show that the annual output of fly ash is about 10,000 kt, and the rational utilization of fly ash has a positive effect on protecting environmental components, such as water and soil, reducing energy consumption and minimizing greenhouse gas emissions. The effect of its application to concrete manufacturing is equivalent to reducing the carbon dioxide emitted by global automobiles by 25% [15].

Slag is a finely ground by-product of slag produced in blast furnaces during steel manufacturing and is effectively used to make mixed mortars, cement, and concrete [16]. It can be used to replace Ordinary Portland Cement (OPC) by up to 35%–70%, and can be used in the production of geopolymer concrete (geopolymer concrete, GPC) [17]. Slag contains Q0-type monosilicate, which is the same as the monosilicate in OPC clinker [18]; it can be used to refine voids during hydration and exhibits high strength and high temperature resistance. In addition, slag can improve concrete resistance to sulfate and alkali-silicon reactions by reducing water demand [12], due to the amorphous nature of irregularly shaped particles, indicating similar reactivity to fly ash. Geopolymers have the advantages of a wide source of raw materials, low production energy consumption, mature technology, fire resistance, chemical corrosion resistance, high mechanical strength, and good durability [19–22]. Researchers have applied geopolymers having good mechanical properties, corrosion resistance, weather resistance, and ease of construction to coatings, thermal insulation materials, fire-resistant and anti-corrosion coatings, and heavy metal solidification [23–25].

In 2014, Masih Mohammadi et al. [26] studied the effect of interfacial binders on the bond strength of repaired concrete, and the effects of FSF15-FMA10 (containing 15% silica fume, 10% metakaolin) and FMB10 (containing 10% metakaolin) were investigated. The results showed that both binders improve the compressive strength of the reinforcement layer at each level, and the stiffness of the overlay layer is increased relative to that of the concrete matrix, resulting in an increase in the shear stress on the contact surface. In addition, because of the low $\text{H}_2\text{O}/\text{Na}_2\text{O}$ molar ratio in the FMB10 type binder, the higher ratio of aluminosilicate has a better reduction effect on calcium hydroxide, which makes the transition zone structure more compact and improves the bond strength. It was concluded that it is reasonable to use the polymer-based binder in concrete repair works in low-humidity environments. Cilla et al. [27,28] conducted experimental studies on the preparation of porous geopolymers with metakaolin, fly ash, and potassium silicate as raw materials and using different surfactants. The results showed that, with the increase in porosity, the permeability increased and the resistance to compressive strength decreased. Nikolicc et al. [29] conducted an experimental study on the curing of Pb by mechanically activated fly ash-based polymers, and the results showed that the geopolymers prepared using mechanically activated fly ash had lower porosity and higher strength. The leaching concentration of Pb is reduced, and the curing effect of Pb is better. In 2016, Alanazi et al. [30] conducted an experimental study on the bond strength of metakaolin-based polymer

mortar for cement concrete pavement repair, and the results showed that the failure of splitting specimens mainly occurred due to interface bond failure. Comparisons with other commercial pavement repair materials show that the metakaolin-based polymer mortar substrate has superior bond strength. The curing time, temperature, and the degradation degree of cement mortar have a significant influence on the interfacial bond strength of geopolymer. The 3-day strength of metakaolinite polymer can reach 80% of that of the 28-day strength, but the strength is lower at 24 h. In 2020, Albidah et al. [31] conducted an experimental study on the bond strength of metakaolin polymer repair mortar and the concrete matrix under normal and high-temperature environments. The results showed that the improvement in the bond strength between the geopolymer repair material and the concrete matrix underwent a significant decrease in the high-temperature exposure environment of 200 °C; however, after the polyvinyl alcohol fibers were mixed into the geopolymer mortar, this occurred at room temperature and a high temperature of 200 °C. The mass ratio of alkali-solid-metakaolin and $\text{Na}_2\text{O}\cdot\text{nSiO}_2\text{-NaOH}$, and the molar ratio of $\text{SiO}_2/\text{Al}_2\text{O}_3$, $\text{H}_2\text{O}/\text{Na}_2\text{O}$ and $\text{Na}_2\text{O}/\text{Al}_2\text{O}_3$, have significant effects on the stability of geopolymer mortar at high temperature.

In this study, the industrial by-product slag and fly ash were used as raw materials, and materials providing green environmental protection and good performance were prepared. The influencing and significance of flexural mechanical properties, and the micro-structure factors, phase composition, and functional group structure of geopolymers under different proportions were analyzed by SEM, XRD, and infrared spectroscopy, showing the effect of different proportions on geopolymer cementitious materials.

2. Materials and Methods

2.1. Materials

2.1.1. Fly Ash

The fly ash used in this test was grade I fly ash produced by Gongyi Borun Refractory Co., Ltd. (Zhengzhou, China). The chemical composition is shown in Table 1. Al_2O_3 and SiO_2 are the main chemical compositions of the fly ash used in this test. The CaO content is only 5.6%, which indicates a low-calcium fly ash that is suitable for the preparation of geopolymers [32]. The particle size of the fly ash is shown in Figure 1.

Table 1. The chemical constituents of fly ash.

Loss on Ignition	Al_2O_3 (%)	SiO_2 (%)	Water (%)	CaO (%)	Alkali (%)	Fe^{3+} (%)	Free CaO (%)	Density (g/cm^3)	Bulk Density (g/cm^3)
2.8	24.2	45.1	0.85	5.6	1.2	0.85	0.85	2.55	1.12

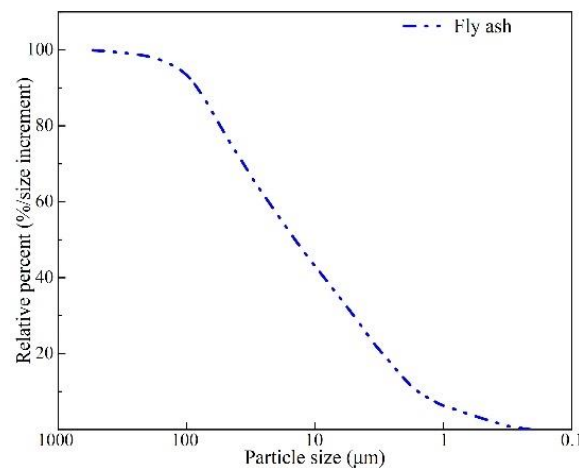


Figure 1. The particle size of the fly ash.

2.1.2. Slag

The slag selected in this experiment was taken from the S95 grade slag powder produced by Henan Borun Foundry Co., Ltd. The vitreous content in the main chemical composition is over 99%. The chemical composition is shown in Table 2. The particle size of the slag is shown in Figure 2.

Table 2. The chemical constituents of slag.

SO ₃	Loss on Ignition	Alkali Content	Vitreous Content	Water Content	Density (g/cm ³)
0.1	0.8	0.56	99	0.1	2.9

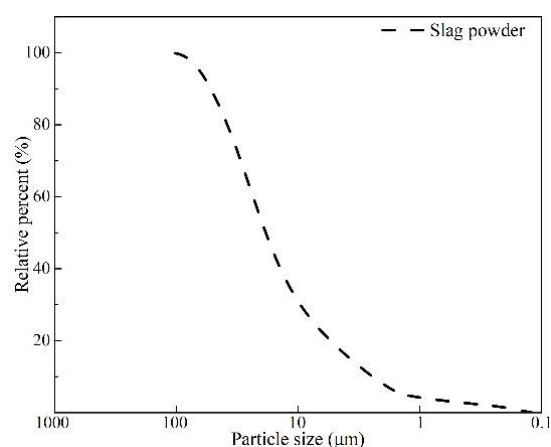


Figure 2. The particle size of the slag.

2.1.3. Alkali Activators

Compared with sodium hydroxide, water glass activator is a complex mixture solution composed of silicate and oxide. The level of water glass modulus ($n(\text{SiO}_2)/n(\text{Na}_2\text{O})$, M) determines the physicochemical properties and mechanical properties, such as the degree of polymerization and molecular structure of each component. The main parameters of the sodium water glass used in this paper are shown in Table 3.

Table 3. Main parameters of sodium silicate.

Modulus (M)	SiO ₂ (%)	NaO (%)	Fe (%)	Density	Water Insoluble Content (%)
3.24	27.45	8.73	0.019	1.38	0.2

2.2. Orthogonal Experimental Design

In this study, the optimal mixing ratio of geopolymer was obtained by the orthogonal test method; the compressive and flexural strength of geopolymers were used as test indicators; and the key factors that have a significant impact on the mechanical properties of geopolymers were obtained in combination with the previous test results. Moreover, the level and combination, including the proportion of slag and fly ash, the modulus of water glass, and the combination of the water-to-binder ratio, were used to control the amount of water glass to 12%. In this study, the design of the experimental Scheme 1 was combined with the actual needs of the application of reinforced impregnating glue, using an orthogonal design table with 5 levels and 6 factors, and using three empty columns as error terms. Considering the above three factors, 25 sets of experimental schemes were carried out. The test factors and levels are shown in Table 4, and the orthogonal test table is shown in Table 5.

Table 4. The factors and levels of tests.

Level	Factor A	Factor B	Factor C
	Slag Mass Fraction (%)	Water-to-Binder Ratio	Water Glass Modulus
1	40	0.36	0.8
2	50	0.38	1.0
3	60	0.40	1.2
4	70	0.42	1.4
5	80	0.44	1.8

Table 5. Orthogonal test L25 (5^3) and test results.

Sample	Compressive Strength (MPa)		Flexural Strength (MPa)	
	7-Day	28-Day	7-Day	28-Day
1	12.3	15.5	0.9	1.7
2	29.3	31.5	2.6	3.5
3	32.5	36.1	4.1	4.2
4	28.1	30.2	3.7	3.5
5	7.8	21.3	1.1	1.8
6	24.1	20.5	3.2	3.3
7	28.6	40.7	3.8	4.9
8	28.8	36.1	4.1	5
9	23.4	20.8	3.7	3.5
10	19.7	24.4	2.8	3.2
11	37.2	43.1	5.2	5.3
12	30.4	34	4.1	4.8
13	26.3	29.4	3.8	4
14	11.5	21.5	1.8	2.8
15	30	31.6	4.1	4.2
16	25.9	40.9	3.7	5.1
17	41.6	61.8	4.4	5.8
18	17.8	29.6	2.7	4.5
19	22.9	33.9	4	4.7
20	28.6	44.5	4.6	6
21	16.9	34.1	2.5	4.3
22	10.3	13.8	1.5	2.3
23	9.6	29.9	1.6	3
24	8.9	46.8	1.6	5.5
25	10.8	27.8	1.7	3.2

2.3. Sample Preparation

Water glass, slag, fly ash, and deionized water were weighed according to the mixing ratio design requirements and poured into the mixing pot. To mix evenly, fast and slow mixing was performed for 4 min according to the automatic mixing program of the NJ-160B cement slurry mixer. The geopolymer slurry was injected into a 40 mm × 40 mm × 160 mm test mold, and placed on a vibrating table for 30 s, and the surface of the test piece was covered with plastic wrap to ensure that the test piece did not experience shrinkage cracks due to water loss during curing. The slurry was placed in a standard curing room (temperature is 20 ± 2 °C, relative humidity is more than 95%) for curing to a specified age for strength testing. Parts were sampled for subsequent microscopic characterization.

2.4. Test Method

2.4.1. Mechanical Properties Testing

The flexural and compressive strength of geopolymer specimens was tested after curing to the test age, as shown in Figures 3 and 4.



Figure 3. Test specimens of flexural and compressive strength of geopolymer.

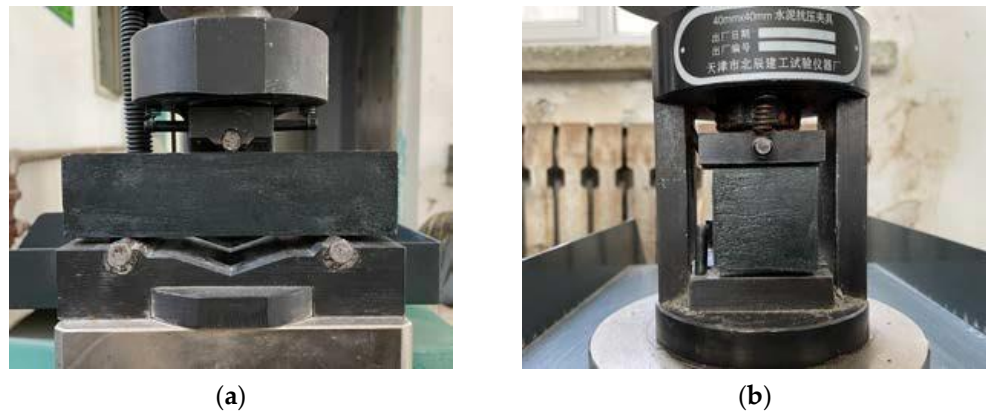


Figure 4. Strength test of geopolymer: (a) flexural strength; (b) compressive strength.

The flexural strength of the specimen is calculated according to Formula (1):

$$R_f = 1.5F_fL/b^3 \quad (1)$$

where R_f is the flexural strength (MPa); F_f is the maximum load at failure (N); L is the distance between the supporting cylinders (mm); b is the side length of the specimen section (mm).

The flexural strength of the specimen is calculated according to Formula (2):

$$R_c = F_c/A \quad (2)$$

where R_c is the compressive strength (MPa); F_c is the maximum load at failure (N); A is the compressive area of the specimen (mm^2).

2.4.2. Orthogonal Test

Orthogonal test schemes are used to optimize the design considering operability, and economical and time costs, when selecting the optimal scheme from among numerous factors and levels of influence. In the orthogonal test, the index refers to the characteristic value of the evaluation test effect according to the test requirements, such as the 7-day and 28-day compressive strength and flexural strength used in this study. Factors refer to different reasons that directly affect the index, which can be expressed as factor A, factor B, and factor C, such as the modulus of water glass, the proportion of slag and fly ash, and water–binder ratio. Level refers to the different values taken by the selected factors due to the change in the state or condition in the test, which are represented by level 1, level 2, etc., such as the three levels of water glass modulus of 0.8, 1.0, and 1.2 in this

study. Orthogonal testing can quickly identify the orthogonality factors and levels from a large number of interfering factors with lower test times, so as to achieve the purpose of significantly reducing test time, and is widely used in production and scientific research. The range analysis method is a commonly used method in the orthogonal test, which intuitively analyzes the order of the influencing factors in the test data; this is also known as the intuitive analysis method. The variance analysis method is used to supplement the range analysis to obtain the size of the test error and improve the accuracy.

2.4.3. Microstructure Testing

In this study, geopolymers of different proportions were selected for curing in a standard environment, the hydration of the samples was terminated with anhydrous ethanol solution, and the test ages of 3, 7, and 28 days were selected to prepare the samples required for scanning electron microscope (SEM) tests, X-ray diffraction system (X-ray) powder diffraction tests, and Fourier transform infrared (FTIR) spectrum analysis.

3. Results and Discussion

3.1. Mechanical Properties Analysis

In this study, the inspection indexes of the geopolymer orthogonal test were mainly the 7-day and 28-day compressive strength and flexural strength, as shown in Table 5.

Polar difference methodology was used to visually analyze the geopolymer strength test results. The 7-day and 28-day compressive and flexural strength results of the orthogonal test were visually analyzed and calculated, as shown in Tables 6 and 7.

Table 6. Range analysis of compressive strength results.

Sample	7-Day Compressive Strength			28-Day Compressive Strength		
	A	B	C	A	B	C
K1	22	23.28	14.32	26.86	30.82	20.82
K2	24.92	28.04	23.18	28.4	36	29.42
K3	27.08	23	27.16	31.9	32.22	42.14
K4	27.36	18.96	24.8	42.1	30.64	33.78
K5	11.3	19.38	23.2	30.34	29.92	33.44
R	16.06	9.08	12.84	15.24	6.08	21.32

Table 7. Range analysis of flexural strength results.

Level	7-Day Flexural Strength			28-Day Flexural Strength		
	A	B	C	A	B	C
K1	2.48	3.1	1.94	2.94	3.94	2.9
K2	3.52	3.28	3.1	3.98	4.26	3.74
K3	3.8	3.26	3.86	4.22	4.14	5.18
K4	3.88	2.96	3.46	5.22	4	4.32
K5	1.78	2.86	3.1	3.66	3.68	3.88
R	2.1	0.42	1.92	2.28	0.58	2.28

K1~K5 in the table respectively represent the average compressive and flexural strength of each factor at levels 1~5; these can reflect the influence of each factor on the mechanical properties at different levels, so as to obtain the optimal level of this factor. R represents extremely poor properties, and reflects the influence of this factor on the mechanical properties when the factor changes at different levels. A larger R indicates that the factor is more important. Conversely, it indicates that the effect of this factor is secondary.

According to Tables 5 and 6, it can be seen that the order of primary and secondary factors affecting the mechanical properties of geopolymers is slag content, water glass modulus, and water-to-binder ratio. The 28-day compressive and flexural strengths are the

main factors. The second order is the modulus of water glass, the amount of slag, and the water-to-binder ratio. This shows that the content of slag and the modulus of water glass have the most significant effects on the compressive strength, and the water–binder ratio has the smallest effect. The level with the largest K value in each factor is the optimal level; that is, the factor level combination of the optimal mix ratio of the geopolymer obtained by the orthogonal test is slag content of 70%, water–binder ratio of 0.38, and water glass modulus of 1.2.

The trend diagrams of slag mass fraction, water-to-binder ratio, water glass modulus, and compressive strength are shown in Figure 5a–c, respectively. Slag mass plots of fractions, water-to-binder ratio, and water glass modulus versus flexural strength are shown in Figure 5d–f, respectively. It can be seen from Figure 5 that the compressive strength and flexural strength show a development trend of increasing first and then decreasing with the increase in the mass fraction of slag, the water–binder ratio, and the modulus of water glass. Adding slag can fill the pores between particles to make it denser and more cohesive, thereby improving the strength; however, when the amount of slag is large, the fluidity of the geopolymer is poor. It can be seen from the test results that adding a small amount of fly ash to the slag not only improves the workability and durability of the geopolymer, but also improves the later strength. The geopolymer slurry is dry and hard, and the mixing property is poor when the water–gel ratio is small. The cementitious materials cannot be mixed sufficiently and uniformly, and the gap between the materials also increases accordingly. These factors directly affect the mechanical properties and workability of geopolymers. In addition, when the water-to-binder ratio is too small, the initial setting time of the geopolymer is too short, which is not suitable for engineering applications. When the water–gel ratio is larger, the strength is reduced and the fluidity is too large to be applied in practical engineering. The main influence of water glass modulus on the performance of the geopolymer is that, the lower the modulus, the higher the alkalinity. In addition, the alkalinity directly affects the degree of dissolution of Si^{4+} and Al^{3+} in the gelling material during the reaction of the geopolymer. Higher alkalinity leads to more soluble Si^{4+} and Al^{3+} in the geopolymer raw material, and greater tendency to a depolymerization reaction [33]. The resulting geopolymer gel is denser and without pores, resulting in a consequent increase in compressive strength.

Although the visual analysis method is intuitive and clear, it also has limitations. Visual analysis cannot assess the size of the error of the experiment. Therefore, it is necessary to perform variance analysis on the orthogonal test results. The results of variance analysis are shown in Tables 8–11. In these tables, the * means $0.01 \leq \text{sig.} < 0.05$, and the ** means $0.001 \leq \text{sig.} < 0.01$.

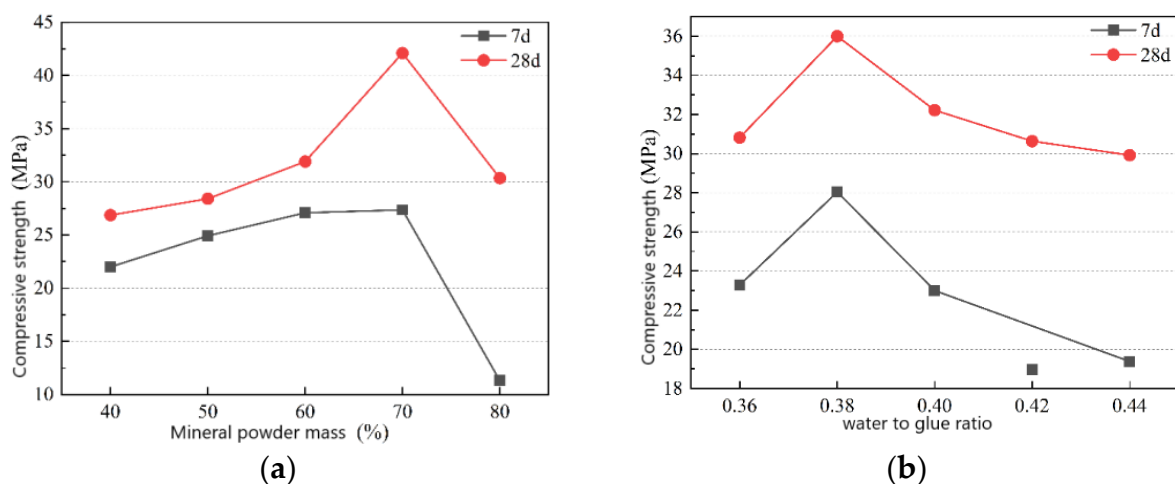


Figure 5. Cont.

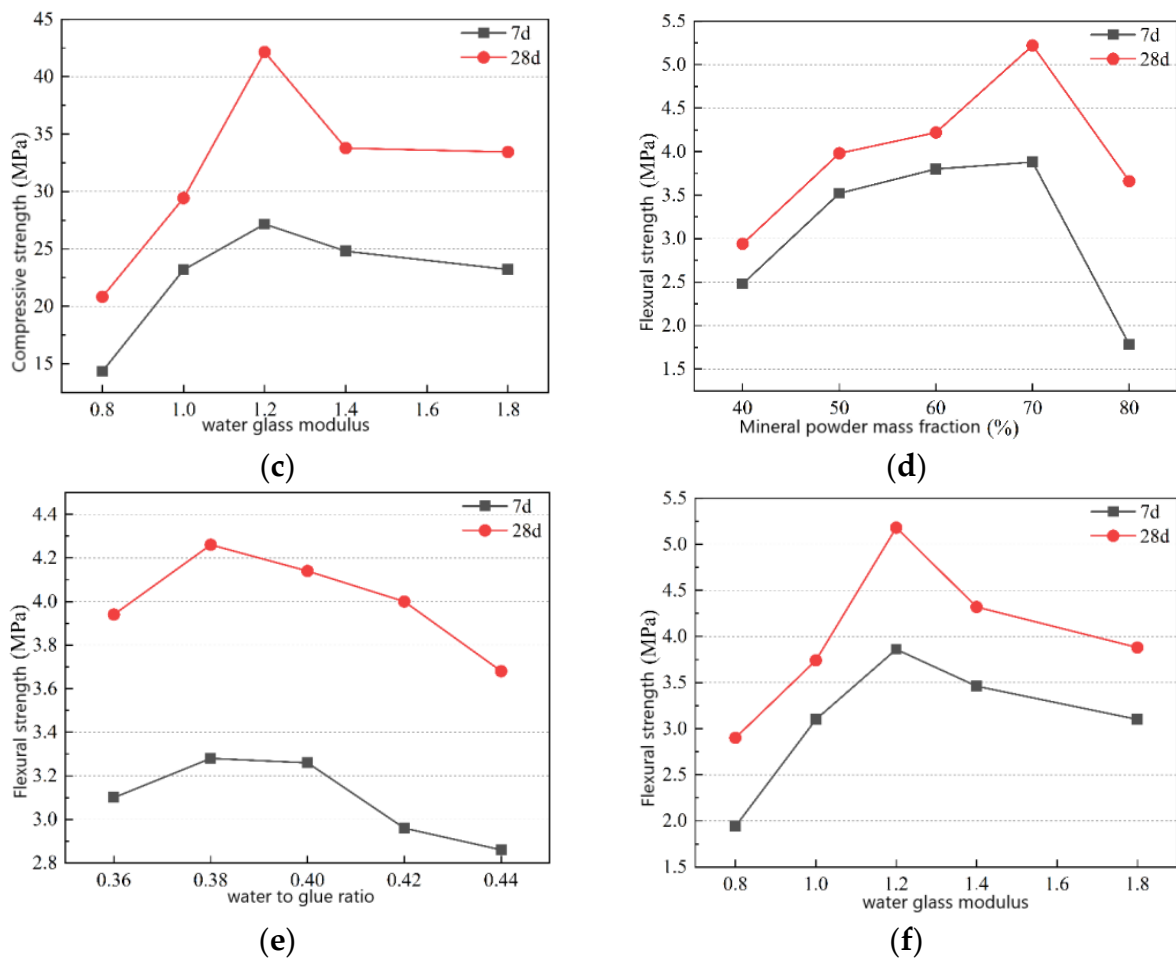


Figure 5. The variance analysis effect curve: (a): slag mass fraction versus compressive strength, (b): water-to-binder ratio versus compressive strength, (c): water glass modulus versus compressive strength, (d): slag mass fraction versus flexural strength, (e): water-to-binder ratio versus flexural strength, (f): water glass modulus versus flexural strength.

Table 8. Variance analysis table of 7-day compressive strength results of orthogonal test.

Factor	Deviation Sum of Squares	Degrees of Freedom	F Value	Fa	Significant Level
Slag mass fraction	880.686	4	17.876	F0.05 (4,4) = 6.39	**
Water-cement ratio	269.054	4	5.461	F0.01 (4,4) = 16	*
Water glass modulus	474.326	4	9.628		
Error	49.27	4			

Table 9. Variance analysis table of 28-day compressive strength results of orthogonal test.

Factor	Deviation Sum of Squares	Degrees of Freedom	F Value	Fa	Significant Level
Slag mass fraction	715.962	4	5.593	F0.05 (4,4) = 6.39	
Water-cement ratio	133.13	4	1.04	F0.01 (4,4) = 16	
Water glass modulus	1192.598	4	9.316		*
Error	128.01	4			

Table 10. Variance analysis table of 7-day flexural strength results of orthogonal test.

Factor	Deviation Sum of Squares	Degrees of Freedom	F Value	Fa	Significant Level
Slag mass fraction	17.006	4	25.845	F0.05 (4,4) = 6.39	**
Water-cement ratio	0.674	4	1.024	F0.01 (4,4) = 16	
Water glass modulus	10.262	4	15.596		*
Error	0.66	4			

Table 11. Variance analysis table of 28-day flexural strength results of orthogonal test.

Factor	Deviation Sum of Squares	Degrees of Freedom	F Value	Fa	Significant Level
Slag mass fraction	13.882	4	15.407	F0.05 (4,4) = 6.39	*
Water-cement ratio	0.966	4	1.072	F0.01 (4,4) = 16	
Water glass modulus	13.934	4	15.465		*
Error	0.9	4			

From Tables 7–10, it can be concluded that, for the compressive and flexural strength of geopolimer at 7 days, the F value of the two factors of slag content and water glass modulus has a confidence level of 95%. When the average time is greater than the F critical value of 6.39, it has reached a significant level. The F value of the slag content is greater than the F critical value of 16 when the confidence level is 99%; that is, it has reached a highly significant level. For the compressive strength of geopolimer at 28 days, the F value of the modulus factor of water glass is greater than the critical F value of 6.39 at a confidence level of 95%. For the flexural strength of geopolimer at 28 days, the F value of the slag mass fraction and water glass modulus factor is greater than the F critical value of 6.39 when the confidence level is 95%, and both reach the significant level. This shows that the results of the geopolimer orthogonal test are reasonable.

3.2. Microscopic Mechanism Analysis

3.2.1. SEM Analysis

The optimal proportion of geopolimer hydration at 3, 7, and 28 days, and the hydration products of Schemes 1 and 2 with an age of 28 days, from scanning, are shown in Figure 6.

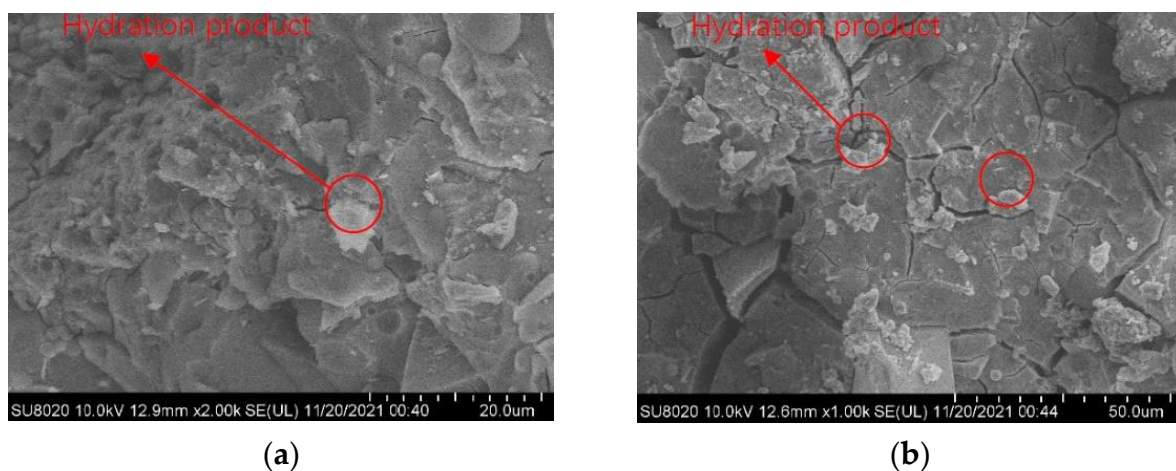


Figure 6. Cont.

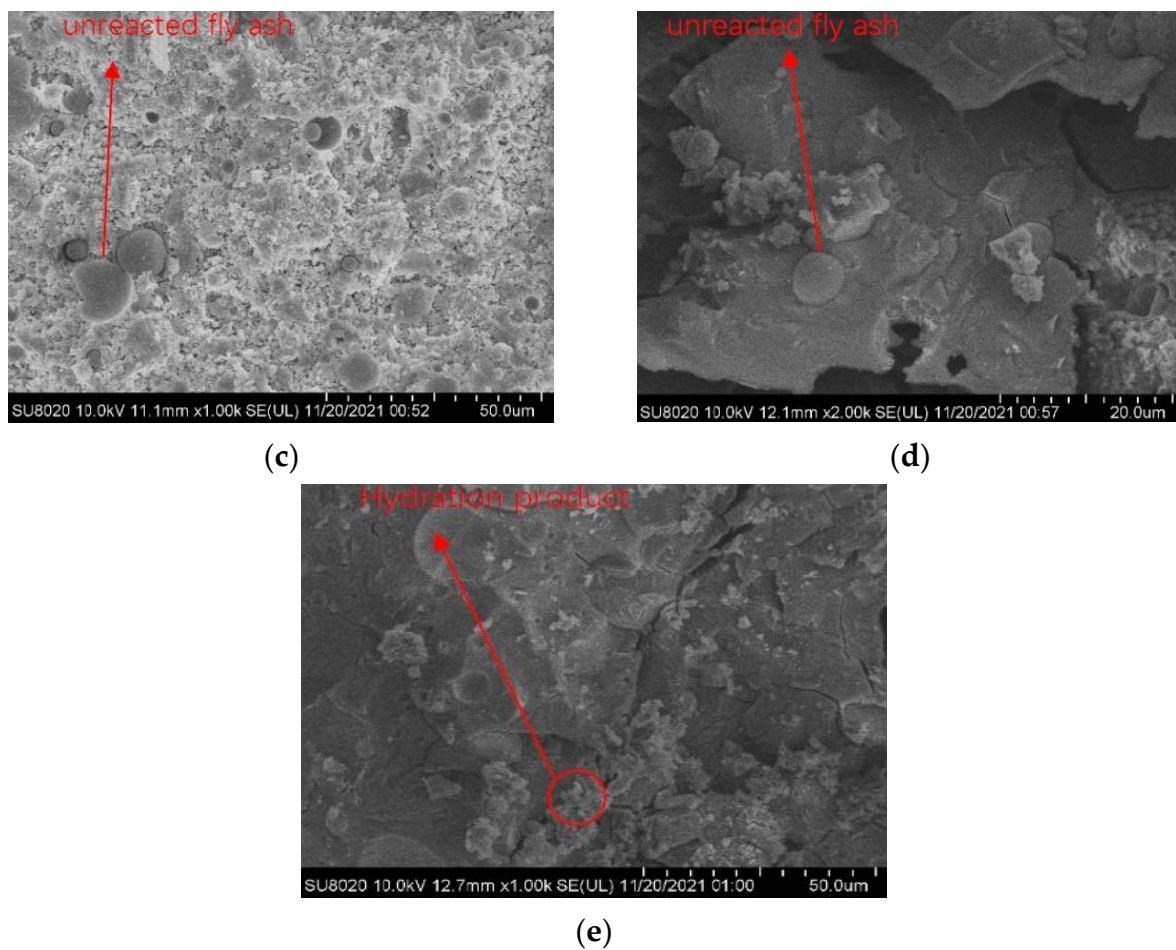


Figure 6. The scanning electron micrographs: (a) 3 days; (b) 7 days; (c) 28 days; (d) Scheme 1; (e) Scheme 2.

The scanning electron microscope images of Schemes 1 and 2 of the optimal mix ratio sample curing for 3, 7, and 28 days, and the control group for curing at 28 days, are shown in Figure 6a–e. By comparing the scanning electron microscope images of the 28-day specimen with the best mix ratio and the 3-day and 7-day specimens, it can be seen that the microstructure of the 3-day and 7-day specimens contains more macropores, and the hydration products formed are relatively coarse and loose. The microstructure of the 28-day specimen is denser, with more gel-like hydration products and fewer pores, indicating that more hydration products are generated with the increase in curing days. As shown in Figure 6c–e, the optimal mix ratio specimen is compared with the specimens of Schemes 1 and 2. Scheme 1 exhibits a few tiny pores and fewer hydration products. In addition, compared with the activity of fly ash, the activity of slag is higher, and the alkali-induced reaction is an exothermic process. The generated heat accelerates the geopolymerization process, which can generate more gel products in a shorter period. This can fill the pores between the particles and make the microstructure denser. It was proven that, with the increase in slag content to 70%, the gel-like hydration products increase significantly, and the mechanical properties improve significantly. However, an excessive amount of slag was shown to cause the drying shrinkage during the maintenance process of the material to increase and the durability to decrease. This phenomenon can be reflected in this test.

3.2.2. XRD Analysis

The XRD analysis of the geopolymer raw material fly ash and slag was carried out, and the X-ray diffraction pattern is shown in Figures 7 and 8. The selection of XRD samples

is consistent with that of SEM samples, and the X-ray diffraction patterns are shown in Figures 9 and 10.

Figure 7 shows the X-ray diffraction pattern of fly ash, whose main components are mullite, calcite, and hematite. Furthermore, the diffraction spectrum of fly ash was quantitatively calculated by Jade software; the content of $\text{Al}_6\text{SiO}_{13}$ was 61.1% and the content of SiO_2 was 38.9%. The bulging peaks in the range of $15\text{--}40^\circ$ in the fly ash spectrum are amorphous mineral phases; as a result, fly ash has the potential of pozzolanic activity. Figure 8 shows the X-ray diffraction pattern of the slag. There is an obvious amorphous phase in the broad peaks between 20° and 40° at 2θ , and the crystallinity is very low, showing that the main phase is an amorphous material, namely, a glassy phase with high potential pozzolanic activity. In addition, it contains a small number of characteristic peaks of mayorite ($\text{Ca}_2\text{AlFeO}_5$), and no other crystal diffraction peaks appear.

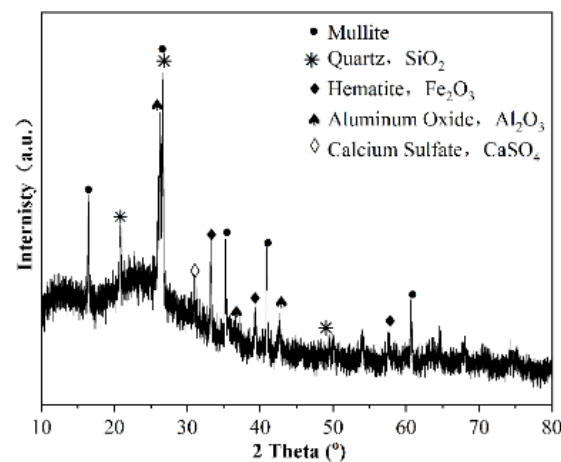


Figure 7. X-ray diffraction pattern of fly ash.

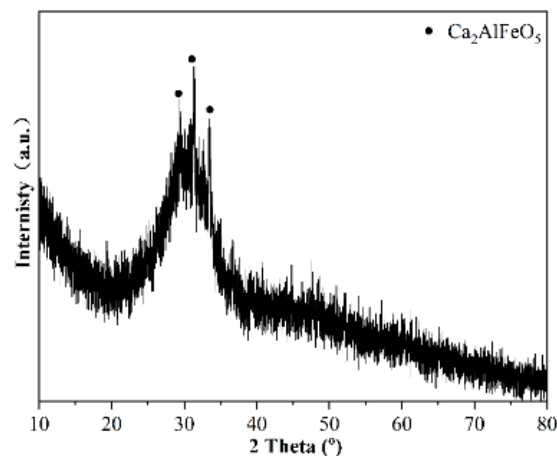


Figure 8. X-ray diffraction pattern of slag powder.

The XRD patterns of the optimal 3-day, 7-day, and 28-day mix ratio specimens are shown in Figure 9. The main mineral compositions of the 3-day, 7-day, and 28-day specimens are hydrated calcium aluminosilicate gel (C-A-S-H), hydrated calcium silicate gel (C-S-H), and RO phase (solid solution of MgO , FeO , and MnO). A clear trend can be found in which the peak intensity at 2θ between 27.2 and 31.2° increases with standing time, indicating an increase in the number of gel products. Figure 10 shows the XRD patterns of the sample with the best mix ratio of Schemes 1 and 2 at 28 days. The 3-day, 7-day, and 28-day main phases are aluminosilicate (C-S-H). Among these, the sample with the best mix ratio at 28 days was compared with Scheme 1; the increase in the slag content leads to

the broadening of the peak between 27.2° to 31.2° , indicating that the amorphous content increases, which is related to the relatively high amorphous content of the slag itself. The strength of the specimen with the best mix ratio at 28 days increased, and the diffraction peak became wider, indicating that the amorphous three-dimensional network structure of aluminosilicate gel increased.

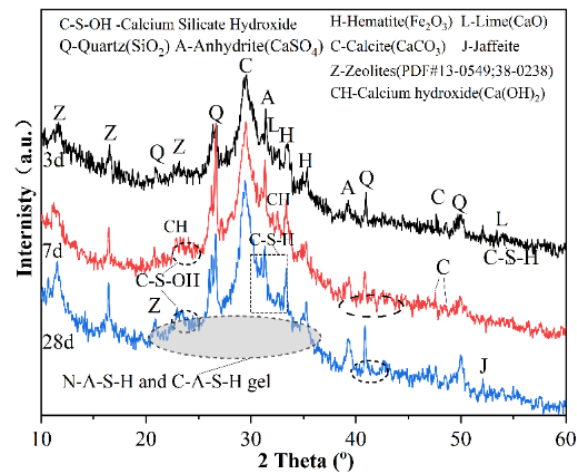


Figure 9. X-ray diffraction patterns of 3-day, 7-day, and 28-day optimal proportioning samples.

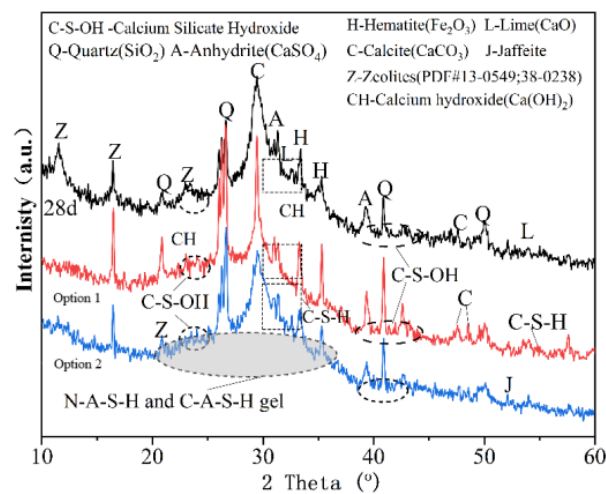


Figure 10. X-ray diffraction patterns of Scheme 1, Scheme 2, and 28-day optimal proportioning sample.

3.2.3. FTIR Analysis

A Spectrum 400 Fourier transform infrared spectrometer of PerkinElmer Company was used to measure the changes in characteristic peaks of geopolymers specimens under the influence of different factors, to study the changes of chemical groups, and to analyze their structures.

As shown in Figure 11, the infrared spectra of fly ash, slag, the 28-day optimum mix ratio specimen, and the 3-days optimum blend ratio specimen are shown. It can be seen from the infrared spectrum of fly ash that there are obvious absorption peaks at 1480 , 1062 , 1003 , 781 , and 594 cm^{-1} , of which the absorption peak at 1480 cm^{-1} is the vibration absorption peak of Mg-O; the absorption peaks near 1062 and 1003 cm^{-1} are the same as the asymmetric stretching vibration peak of Al(Si)-O-Si; 781 cm^{-1} is the symmetrical stretching vibration of Si-O; and the bending vibration peak of Al-O-Si is near 594 cm^{-1} .

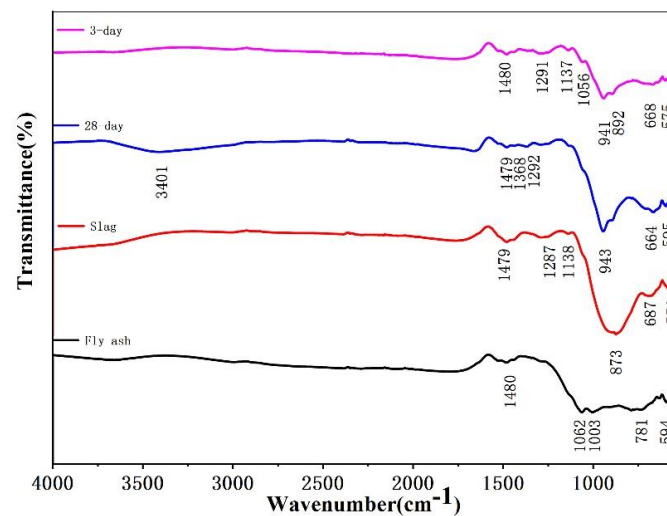


Figure 11. Infrared spectrum of slag, fly ash, and optimum mix proportion test specimens at different ages.

In the infrared spectrum of the slag, the Mg-O vibrational absorption peak also appears near 1479 cm^{-1} ; the absorption peaks at 1287 cm^{-1} and 1138 cm^{-1} are Al(Si)-O-Si and Si-O, respectively. The stronger absorption peak at 873 cm^{-1} is the Si-O asymmetric stretching vibration peak; 687 cm^{-1} is related to the vibration of O-Si-O; the absorption peak at 556 cm^{-1} is related to Al-O-Si bending vibration peaks. In the infrared spectra of the 3-day and 28-day samples having the best mix ratio, there are relatively strong and broad absorption peaks around 940 cm^{-1} , and the absorption peaks here are generated by the Si-O stretching vibration of water glass. This indicates that the Si in slag and fly ash forms a network connection with Si in water glass, and the strength of 28-day is significantly greater than that of 3-day, indicating that the increase in curing days is beneficial to the formation of the Al(Si)-O-Si network structure.

As shown in Figure 12, in the infrared spectrum of Scheme 2, the Si-O stretching vibration peak near 942 cm^{-1} is significantly lower than the infrared spectrum of the best mix ratio specimen. The O content is relatively increased, indicating that the appropriate water glass modulus and fly ash content are beneficial to the formation of the Al(Si)-O-Si network. In the infrared spectrum of Scheme 1, it can also be seen that the Si-O stretching vibration peak near 942 cm^{-1} is significantly lower than the infrared spectrum of the optimal mixture ratio specimen, indicating that the Si-O content of the optimal mixture ratio specimen is high. In Scheme 1, the increase in the water glass modulus and the water-to-binder ratio content is beneficial to the formation of the Al(Si)-O-Si network.

According to the analysis results of the chemical composition and infrared spectrum of the geopolymer, the reaction mechanism of the alkali-excited geopolymer prepared from low-calcium aluminosilicate includes two main stages: dissolution-depolymerization and recombination-polycondensation [34,35]. The schematic diagram of the reaction mechanism is shown in Figure 13 [36].

First, the chemical bonds of aluminosilicate raw materials such as fly ash, slag, and metakaolin are broken under the action of alkali excitation, and are decomposed into a silicon-oxygen tetrahedron $[\text{SiO}_4]^{4-}$ and aluminum-oxygen tetrahedron $[\text{AlO}_4]^{5-}$ monomer. As the dissolution progresses, the monomers connect to each other to form dimers, and the dimers react with other monomers to form trimers or multimers. The monomers are finally polycondensed into amorphous sodium aluminosilicate hydrate (N-A-S-H) gels having a three-dimensional network structure. In the early stage of the reaction, when the reaction reaches saturation, the dissolution rate of Al is faster than that of Si in the aluminosilicate minerals under alkaline conditions, resulting in a relatively high content of Al^{3+} . Consequently, metastable Al-rich N-A-S-H gels (Si/Al ratio $\cong 1.0$ – 1.3 , Al-rich gel I) are increased and precipitated as intermediates [37]. As the reaction proceeds, more Si-O groups dissolve, increasing the concentration of Si^{4+} in solution and its ratio in

N-A-S-H-gel (Si/Al ratio $\cong 2$, silica-rich gel II). This structural reorganization determines the final composition of the polymer's three-dimensional network structure consisting of a silicon-alumina framework and charge-balancing metal cations, in addition to the pore structure and distribution in the material.

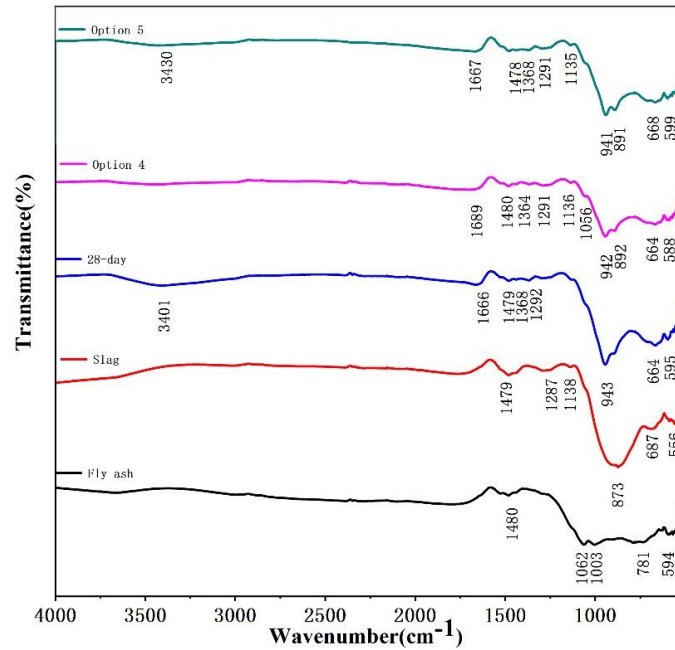


Figure 12. Infrared spectrum of slag, fly ash, and differential mix proportion test specimens.

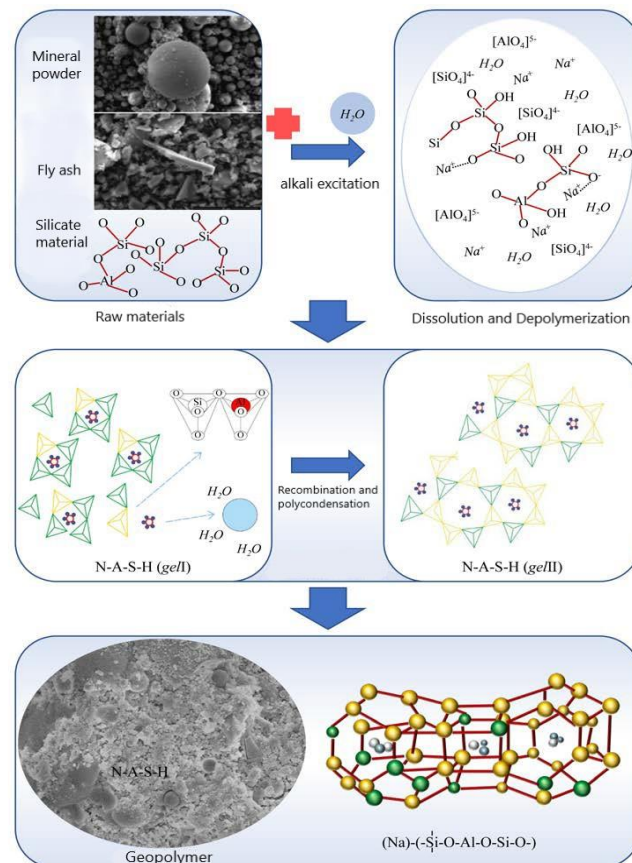


Figure 13. The schematic diagram of reaction mechanism.

Based on the silicon-aluminum ratio (Si/Al) reaction product, Davidovits geopolymer structures are classified into three types: Poly sialate (PS) (-Si-O-Al-), Poly sialate-siloxo (PSS) (-Si-O-Al-O-Si-) and Poly sialate-disiloxo organization (-Si-O-Al-O-Si-O-Si-) [38]. Accordingly, the molecular formula of the geopolymer can be expressed as $Mn(-SiO_2)_z-AlO_2-n \cdot wH_2O$, where z is 1, 2, or 3; M is an alkali metal (Na^+ , K^+ , etc.); n is the degree of polymerization; and w is the bound water content. The geopolymers prepared from high calcium aluminum silicate materials (high calcium fly ash, etc.) have two gel products, namely, sodium silicate hydrate (N-A-S-H) and calcium silicate hydrate (C-S-H). Moreover, in some cases, when Al^{3+} replaces Si^{4+} in C-S-H, C-S-H is converted to C-A-S-H [39]. High temperature can enhance kinetic energy and thus increase the effect of solute molecules to break bonds through solvent molecular and intermolecular gravitational forces [40]. When the activator is below a certain level, several aluminosilicate precursors are left unreacted due to the lack of a medium for the reaction to take place [41]. In addition, it was found that the gel structure of the geopolymer is similar to that of the zeolite, but the geopolymer has a relatively dense amorphous or semi-crystalline mesoporous structure, whereas natural zeolites are usually crystalline. This may be due to the rapid dissolution of the glass component when the aluminosilicate material is mixed with the alkaline solution. In this case, the gel does not have enough time and space to grow into a well-crystallized structure, resulting in the formation of microcrystalline, amorphous, or semi-crystalline structures. In addition, according to the research of Provis [42], geopolymers are divided into low-calcium and high-calcium systems according to the CaO content in the raw materials. The low-calcium system is a three-dimensional network structure (N-A-S-H gel structure) having low strength. The fly ash in this paper provides more CaO content for the geopolymer, forming a high calcium system (layered (C-(A)-S-H gel structure) having higher strength.

4. Conclusions

Through the orthogonal test, the best mix ratio of the geopolymer was optimized with the compressive strength and flexural strength as the evaluation criteria, and the microstructure and mechanical properties of the geopolymer were studied. Based on the test results, the following conclusions are drawn:

1. The influence factors of compressive and flexural strength of geopolymers were analyzed using the orthogonal test, and it was found that the content of slag and the modulus of water glass had significant effects on the mechanical properties of 7-day and 28-day geopolymers, respectively. The geopolymers prepared at room temperature were obtained. The compressive and flexural strengths of the polymer can reach 65.3 and 6.1 MPa, respectively.
2. The calculation results based on the range analysis of the orthogonal test show that geopolymer has high early strength and can rapidly improve the reinforcement performance as an impregnating glue. The water-binder ratio and the amount of slag have a significant influence on the constructability of the geopolymer. Selecting the appropriate mixing ratio can yield a geopolymer with good working performance and suitable fluidity. Therefore, the optimal mixing ratio was selected in the follow-up study: the content of slag was 70%, the water-binder ratio was 0.38, and the modulus of water glass was 1.2.
3. The microscopic morphology and phase composition of the geopolymer were analyzed by SEM, XRD, and FTIR. It was determined that the main final product of the geopolymer was hydrated silicic acid, which contributed the most to the development of the early strength of the geopolymer, including calcium gel and hydrated calcium aluminosilicate gel, tetra calcium ferro aluminate mineral, and RO phase.

Author Contributions: Investigation, software, writing—original draft preparation, G.Y.; supervision, Y.J. All authors have read and agreed to the published version of the manuscript.

Funding: The research in this paper was supported by the Natural Science Foundation of Heilongjiang Province of China: Study on the relationship between and macroscopic properties of concrete gel slurry (grant no. E2017003).

Institutional Review Board Statement: Not applicable.

Informed Consent Statement: Not applicable.

Data Availability Statement: No new data were created or analyzed in this study. Data sharing is not applicable to this article.

Conflicts of Interest: The authors declare no conflict of interest.

References

1. Fan, F.; Liu, Z.; Xu, G.; Peng, H.; Cai, C. Mechanical and thermal properties of fly ash based geopolymers. *Constr. Build. Mater.* **2018**, *160*, 66–81. [\[CrossRef\]](#)
2. Padmakar, K.C.; Kumar, B.S.C. An experimental study on metakaolin and GGBS based geopolymer concrete. *Int. J. Civ. Eng. Technol.* **2017**, *8*, 544–557.
3. Xu, H.; Van Deventer, J. The geopolymerisation of alumino-silicate minerals. *Int. J. Miner. Process.* **2000**, *59*, 247–266. [\[CrossRef\]](#)
4. Davidovits, J.; Comrie, D. Long term durability of hazardous toxic and nuclear waste disposals. *Proc. Geopolym.* **1988**, *1*, 125–134.
5. Temuujin, J.; van Riessen, A.; MacKenzie, K. Preparation and characterisation of fly ash based geopolymer mortars. *Constr. Build. Mater.* **2010**, *24*, 1906–1910. [\[CrossRef\]](#)
6. Burciaga-Díaz, O.; Magallanes-Rivera, R.; Escalante-García, J. Alkali-activated slag-metakaolin pastes: Strength, structural, and microstructural characterization. *J. Sustain. Cem. Mater.* **2013**, *2*, 111–127. [\[CrossRef\]](#)
7. Glukhovskij, V.; Zaitsev, Y.; Pakhomov, V. Slag-alkaline cements and concretes-structure, properties, technological and economical aspects of the use. *Silic. Ind.* **1983**, *48*, 197–200.
8. Geng, J.; Zhou, M.; Li, Y.; Chen, Y.; Han, Y.; Wan, S.; Zhou, X.; Hou, H. Comparison of red mud and coal gangue blended geopolymers synthesized through thermal activation and mechanical grinding reactivation. *Constr. Build. Mater.* **2017**, *153*, 185–192. [\[CrossRef\]](#)
9. Niklić, I.; Marković, S.; Janković-Častvan, I.; Radmilović, V.V.; Karanović, L.; Babić, B.; Radmilović, V.R. Modification of mechanical and thermal properties of fly ash-based geopolymer by the incorporation of steel slag. *Mater. Lett.* **2016**, *176*, 301–305. [\[CrossRef\]](#)
10. Soutsos, M.; Boyle, A.P.; Vinai, R.; Hadjierakleous, A.; Barnett, S. Factors influencing the compressive strength of fly ash based geopolymers. *Constr. Build. Mater.* **2016**, *110*, 355–368. [\[CrossRef\]](#)
11. Anuradha, R.; Thirumala, R.; John, P.N. Optimization of molarity on workable self-compacting geopolymer concrete and strength study on SCGC by replacing fly ash with silica fume and GGBFS. *Int. J. Adv. Struct. Geotech. Eng.* **2014**, *3*, 11–18.
12. Castel, A.; Foster, S.J. Bond strength between blended slag and Class F fly ash geopolymer concrete with steel reinforcement. *Cem. Concr. Res.* **2015**, *72*, 48–53. [\[CrossRef\]](#)
13. Mantese, G.C.; Amaral, D.C. Comparison of industrial symbiosis indicators through agent-based modeling. *J. Clean. Prod.* **2017**, *140*, 1652–1671. [\[CrossRef\]](#)
14. Wongsas, A.; Siri wattanakarn, A.; Nuaklong, P.; Sata, V.; Sukontasukkul, P.; Chindaprasirt, P. Use of recycled aggregates in pressed fly ash geopolymer concrete. *Environ. Prog. Sustain. Energy* **2019**, *39*, e13327. [\[CrossRef\]](#)
15. Poudenx, P. The effect of transportation policies on energy consumption and greenhouse gas emission from urban passenger transportation. *Transp. Res. Part A Policy Pract.* **2008**, *42*, 901–909. [\[CrossRef\]](#)
16. Puertas, F.; Martínez-Ramírez, S.; Alonso, S.; Vázquez, T. Alkali-activated fly ash/slag cements: Strength behaviour and hydration products. *Cem. Concr. Res.* **2000**, *30*, 1625–1632. [\[CrossRef\]](#)
17. Kelham, S.; Damtoft, J.; Talling, B. The influence of high early-strength (HES) mineralized clinker on the strength development of blended cements containing fly ash, slag, or ground limestone. *Spec. Publ.* **1995**, *153*, 229–248.
18. Babu, K.G.; Kumar, V.S.R. Efficiency of GGBS in concrete. *Cem. Concr. Res.* **2000**, *30*, 1031–1036. [\[CrossRef\]](#)
19. Aiken, T.A.; Kwasny, J.; Sha, W.; Soutsos, M.N. Effect of slag content and activator dosage on the resistance of fly ash geopolymer binders to sulfuric acid attack. *Cem. Concr. Res.* **2018**, *111*, 23–40. [\[CrossRef\]](#)
20. Aliques-Granero, J.; Tognonvi, M.T.; Tagnit-Hamou, A. Durability study of AAMs: Sulfate attack resistance. *Constr. Build. Mater.* **2019**, *229*, 117100. [\[CrossRef\]](#)
21. Lahoti, M.; Tan, K.H.; Yang, E.-H. A critical review of geopolymer properties for structural fire-resistance applications. *Constr. Build. Mater.* **2019**, *221*, 514–526. [\[CrossRef\]](#)
22. Shill, S.K.; Al-Deen, S.; Ashraf, M.; Hutchison, W. Resistance of fly ash based geopolymer mortar to both chemicals and high thermal cycles simultaneously. *Constr. Build. Mater.* **2019**, *239*, 117886. [\[CrossRef\]](#)
23. Abdel-Ghani, N.T.; Elsayed, H.A.; AbdelMoied, S. Geopolymer synthesis by the alkali-activation of blastfurnace steel slag and its fire-resistance. *HBRC J.* **2018**, *14*, 159–164. [\[CrossRef\]](#)
24. Ferone, C.; Roviello, G.; Colangelo, F.; Cioffi, R.; Tarallo, O. Novel hybrid organic-geopolymer materials. *Appl. Clay Sci.* **2013**, *73*, 42–50. [\[CrossRef\]](#)

25. Wang, K.-T.; Tang, Q.; Cui, X.-M.; He, Y.; Liu, L.-P. Development of near-zero water consumption cement materials via the geopolymerization of tektites and its implication for lunar construction. *Sci. Rep.* **2016**, *6*, 29659. [[CrossRef](#)]
26. Mohammadi, M.; Moghtadaei, R.M.; Samani, N.A. Influence of silica fume and metakaolin with two different types of interfacial adhesives on the bond strength of repaired concrete. *Constr. Build. Mater.* **2014**, *1*, 141–150. [[CrossRef](#)]
27. Cilla, M.S.; Colombo, P.; Morelli, M.R. Geopolymer foams by gelcasting. *Ceram. Int.* **2014**, *40*, 5723–5730. [[CrossRef](#)]
28. Cilla, M.S.; Morelli, M.R.; Colombo, P. Effect of process parameters on the physical properties of porous geopolymers obtained by gelcasting. *Ceram. Int.* **2014**, *40*, 13585–13590. [[CrossRef](#)]
29. Nikolić, V.; Komljenović, M.; Marjanović, N.; Baščarević, Z.; Petrović, R. Lead immobilization by geopolymers based on mechanically activated fly ash. *Ceram. Int.* **2014**, *40*, 8479–8488. [[CrossRef](#)]
30. Alanazi, H.; Yang, M.; Zhang, D.; Gao, Z. Bond strength of PCC pavement repairs using metakaolin-based geopolymer mortar. *Cem. Concr. Compos.* **2016**, *65*, 75–82. [[CrossRef](#)]
31. Albidah, A.; Abadel, A.; Alrshoudi, F.; Altheeb, A.; Abbas, H.; Al-Salloum, Y. Bond strength between concrete substrate and metakaolin geopolymer repair mortars at ambient and elevated temperatures. *J. Mater. Res. Technol.* **2020**, *9*, 10732–10745. [[CrossRef](#)]
32. Fernández-Jiménez, A.; Palomo, A. Characterisation of fly ashes. Potential reactivity as alkaline cements. *Fuel* **2003**, *82*, 2259–2265. [[CrossRef](#)]
33. Khale, D.; Chaudhary, R. Mechanism of geopolymerization and factors influencing its development: A review. *J. Mater. Sci.* **2007**, *42*, 729–746. [[CrossRef](#)]
34. Hu, Z.; Wyrzykowski, M.; Lura, P. Estimation of reaction kinetics of geopolymers at early ages. *Cem. Concr. Res.* **2020**, *129*, 105971. [[CrossRef](#)]
35. Palomo, Á.; Kavalerova, E.; Fernández-Jiménez, A.; Krivenko, P.; García-Lodeiro, I.; Maltseva, O. A review on alkaline activation: New analytical perspectives. *Mater. Constr.* **2014**, *64*, e022. [[CrossRef](#)]
36. Zhao, J.; Tong, L.; Li, B.; Chen, T.; Wang, C.; Yang, G.; Zheng, Y. Eco-friendly geopolymer materials: A review of performance improvement, potential application and sustainability assessment. *J. Clean. Prod.* **2021**, *307*, 127085. [[CrossRef](#)]
37. Shi, C.; Roy, D.; Krivenko, P. *Alkali-Activated Cements and Concretes*; CRC press: Boca Raton, FL, USA, 2003.
38. Davidovits, J. Geopolymers: Inorganic polymeric new materials. *J. Therm. Anal. Calorim.* **1991**, *37*, 1633–1656. [[CrossRef](#)]
39. García-Lodeiro, I.; Palomo, A.; Fernández-Jiménez, A.; Macphee, D. Compatibility studies between NASH and CASH gels. Study in the ternary diagram $\text{Na}_2\text{O}-\text{CaO}-\text{Al}_2\text{O}_3-\text{SiO}_2-\text{H}_2\text{O}$. *Cem. Concr. Res.* **2011**, *41*, 923–931. [[CrossRef](#)]
40. Kuenzel, C.; Ranjbar, N. Dissolution mechanism of fly ash to quantify the reactive aluminosilicates in geopolymerisation. *Resour. Conserv. Recycl.* **2019**, *150*, 104421. [[CrossRef](#)]
41. Ranjbar, N.; Kuenzel, C.; Spangenberg, J.; Mehrali, M. Hardening evolution of geopolymers from setting to equilibrium: A review. *Cem. Concr. Compos.* **2020**, *114*, 103729. [[CrossRef](#)]
42. Provis, J.; Myers, R.; White, C.; Rose, V.; van Deventer, J.S. X-ray microtomography shows pore structure and tortuosity in alkali-activated binders. *Cem. Concr. Res.* **2012**, *42*, 855–864. [[CrossRef](#)]